Integrity Analysis for Greedy Search Based Fault Exclusion with a Large Number of Faults

Chen Zhu*, Michael Meurer*, Mathieu Joerger†

*Institute of Communications and Navigation, German Aerospace Center (DLR), Oberpfaffenhofen, Germany
Email: Chen.Zhu@dlr.de, Michael.Meurer@dlr.de

† Aerospace and Ocean Engineering Department, Virginia Tech, Blacksburg, VA, USA
Email: joerger@vt.edu

***Abstract*— Detection and exclusion can be achieved using Solution Separation (SS), for example, in civilian aviation applications using Advanced Receiver Autonomous Integrity Monitoring (ARAIM). Global Navigation Satellite Systems (GNSS) fault modes, which are well defined with predictable probabilities of occurrence, can be efficiently and exhaustively accounted for by grouping. However, other navigation applications emerge that require multi-sensor fusion in varying operational environments. Both the total number of measurements and the number of potentially faulty measurements can increase significantly. For such applications, an exhaustive account of all modes can be challenging and can become computationally intractable. These challenges can be addressed using greedy-search-based fault exclusion. However, methods are lacking to quantify the navigation integrity performance of such approaches. In this research, we perform a theoretical analysis of the integrity of greedy-search-based fault exclusion approach. The methods to calculate the minimal detectable bias and the worst case fault direction are discussed.**

I. Introduction

The emergence of new applications such as vertical take-off and landing (VTOL) of unmanned air vehicle (UAV) set increasingly stringent requirements on navigation systems. Future safety-of-life applications, such as urban air mobility (air-taxis) or self-driving cars, require both high-accuracy and high-integrity solutions.Global Navigation Satellite Systems (GNSS) are instrumental in such applications.Tracking multiple constellations provides advanced GNSS receivers with sufficient satellites to estimate the position accurately, but it may also bring more challenges to monitor the integrity in real time due to higher computational complexity. In addition, the satellite-only solutions face performance degradations in urban environments due to shadowing from tall buildings, strong multipath signals and radio interference. In many cases, multi-sensor solutions are applied to achieve better performance. However, integrity monitoring of multi-sensor navigation solutions is not as mature as for GNSS integrity and faces new challenges, especially when perception sensors such as lidar or cameras are also used for navigation purposes [1], [2]. Monitoring the integrity of the output of navigation systems is therefore more challenging for these new applications. Fig. 1 shows a UAV landing scenario as example. The vehicle positions itself using both the satellite signals and visual features from a georeferenced landing pad.

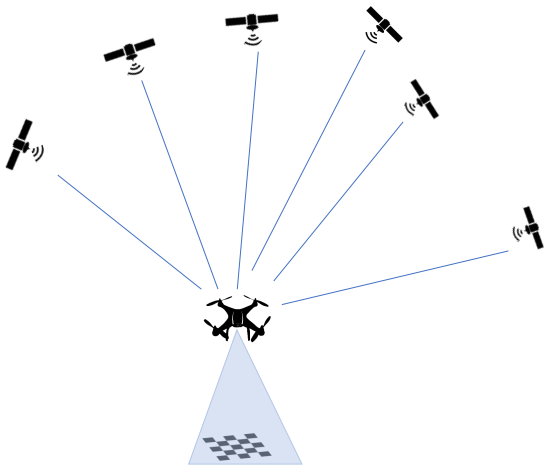

Fig. 1: Simulation scenario of UAV landing

The GNSS integrity monitoring techniques have been developed over the past decades, and play an important role in safety-critical civil aviation applications. Multiple Hypotheses Solution Separation (MHSS) [3], [4] based method is proposed to exclude the faulty measurements and calculate the protection level with convenience. It becomes a state-of-the-art approach for fault detection and integrity monitoring and is applied in advanced Receiver Autonomous Integrity Monitoring (ARAIM) services [5]. The method decomposes the possible combinations of faulty measurements into different hypotheses, and builds a test statistic using the full set of measurements and the fault-tolerant subset for each hypothesis. As a result, the faulty measurements can be detected and isolated according to the statistical test results. The computational complexity of the fault detection and exclusion (FDE) depends on the number of fault modes to be monitored. For multiple faults, the number of fault modes is determined by the prior error rate and the total number of measurements, which can be significantly higher for multi-sensor solutions than for GNSS-only solutions. Consequently, an exhaustive search over all the possible fault modes may become infeasible for real-time monitoring if the computational power does not allow it in some use cases.

To reduce the computational complexity, suboptimal meth-

ods such as greedy search based fault exclusion are proposed [6][7]. The method has been shown to be fast and functional in practice [7]. However, to the best of our knowledge, there is very limited number of literature focusing on the integrity performance of the suboptimal methods. There is some discussion of the integrity for the greedy search based approach in our previous work [8], but only on a preliminary level. In this work, we perform a more extensive theoretical analysis of the integrity aspects of the greedy search based fault exclusion method (referred to as Greedy-FDE in the following sections for convenience).

The paper is organized as follows: in Section II, a general system model is described, and the motivation for using Greedy-FDE for multi-sensor applications is stated. In Section III, the Greedy-FDE method is reviewed and its integrity aspects are analyzed. A numerical problem in multi-sensor navigation and its impact on Greedy-FDE are discussed in Section IV. The analysis is followed by preliminary simulations in Section V to validate the theoretical analysis of the integrity aspects.

II. System Model and Complexity Issue

A. Generalized System Model

In this work, we use bold letters to denote matrices (uppercase) and vectors (lowercase). $\|\cdot\|_2$ denotes the 2-norm (Euclidean norm) of a vector, and $\|\cdot\|_0$ is used to describe the number of non-zero entries of a vector.

Without loss of generality, the measurement equation of a navigation system can be written as

$$\rho = \mathbf{h}(\mathbf{x}) + \mathbf{n} + \mathbf{b}, \tag{1}$$

where $\rho \in \mathbb{R}^N$ is the raw measurement vector from the sensors, $\mathbf{x} \in \mathbb{R}^M$ is the state vector (including position, clock offset, etc.), $\mathbf{n}$ is the stochastic noise with covariance Σ_n, and $\mathbf{b}$ is the bias vector induced by faults, which is defined as outliers with unpredictable large errors. The main focus of this paper is on fault detection, not nominal bias, so for the rest of the paper, it is assumed that the integrity problems caused by nominal biases are handled by other methods and $\mathbf{b}$ contains only measurement faults. In the multi-sensor context, the vector function between the position and the measurements $\mathbf{h}(\cdot)$ is generally nonlinear. Here it is assumed that the position is estimated in a snapshot-based manner using the Gauss-Newton iterative optimization algorithm (or similarly the Levenberg-Marquardt algorithm [9]), and the convergence of the iterative algorithm is beyond the scope of this work.

Consequently, the measurement equation can be approximated by first-order linearization close to the convergence point:

$$\rho \approx \mathbf{h}(\mathbf{x}_l) + \left.\frac{\partial \mathbf{h}(\mathbf{x})}{\partial \mathbf{x}}\right|_{\mathbf{x}=\mathbf{x}_l} (\mathbf{x} - \mathbf{x}_l) + \mathbf{n} + \mathbf{b}. \tag{2}$$

The linearized measurement equation at point $\mathbf{x}_l$ can be written as

$$\mathbf{z} = \mathbf{H}\mathbf{x} + \mathbf{n} + \mathbf{b} = \begin{bmatrix} \mathbf{J}_{s_1} \\ \vdots \\ \mathbf{J}_{s_k} \end{bmatrix} \mathbf{x} + \mathbf{n} + \mathbf{b}, \tag{3}$$

where $\mathbf{z} = \rho - \mathbf{h}(\mathbf{x}_l) + \mathbf{H}\mathbf{x}_l$. $\mathbf{H}$ is the observation matrix (also known as geometry matrix in satellite navigation), which is the stack of Jacobian matrices from all the k sensors.

For GNSS pseudorange measurements, the state vector $\mathbf{x} = [\mathbf{p}, \mathbf{c}]$, which consists of the receiver position and the clock offset. For simplicity, we assume a single constellation here, so that the clock is a scalar. The Jacobian matrix can be calculated by

$$\mathbf{J}_{GNSS} = \begin{bmatrix} \frac{\mathbf{p}-\mathbf{p}^1_{sat})^T}{\|\mathbf{p}-\mathbf{p}^1_{sat}\|} & 1 \\ \vdots & \\ \frac{\mathbf{p}-\mathbf{p}^K_{sat})^T}{\|\mathbf{p}-\mathbf{p}^K_{sat}\|} & 1 \end{bmatrix}, \tag{4}$$

where $\mathbf{p}^i_{sat}$ denotes the position of the i-th satellite.

The measurement equation of a camera for the m-th landmark point is

$$\begin{aligned} \mathbf{z}^m_{cam} &= \pi_m(\mathbf{p}) + \mathbf{n}^m_{cam} + \mathbf{b}^m_{cam} \\ &= \frac{\begin{bmatrix} 1 & 0 & 0 \\ 0 & 1 & 0 \end{bmatrix} \mathbf{K}\mathbf{R}^T(\mathbf{p}^m_{map} - \mathbf{p})}{\begin{bmatrix} 0 & 0 & 1 \end{bmatrix} \mathbf{K}\mathbf{R}^T(\mathbf{p}^m_{map} - \mathbf{p})} + \mathbf{n}^m_{cam} + \mathbf{b}^m_{cam}, \end{aligned} \tag{5}$$

where $\mathbf{p}^m_{map}$ denotes the landmark position and the camera attitude is expressed by $\mathbf{R} \in \mathrm{SO}(3)$. $\mathbf{K}$ is the intrinsic matrix which transforms the position information in the camera local frame to pixel location in the image.

The least squares solution from the iterative optimization is denoted as

$$\hat{\mathbf{x}} = \mathbf{S}\mathbf{z} = \left(\mathbf{H}^T\mathbf{W}\mathbf{H}\right)^{-1}\mathbf{H}^T\mathbf{W}\mathbf{z} \tag{6}$$

with $\mathbf{W} = \Sigma_n^{-1}$ assuming that $\mathbf{n} \sim N(\mathbf{0}, \Sigma_n)$.

B. Maximum Number of Faults

For solution separation based integrity monitoring using multiple hypotheses statistical test, the null hypothesis $\mathscr{H}_0$ assumes that all the N measurements are bias-free. Alternative hypotheses correspond to all the possible combinations of the faulty measurement indices. For exactly N_f faulty measurements, there are $\mathrm{C}^{N_f}_{N_p}$ (choose N_f from N_p) alternative hypotheses. Therefore, if there are at most $N_{f,max}$ faults to monitor, the total number of alternative hypotheses is

$$N_{\text{mode}} = \sum_{N_f=1}^{N_{f,max}} \mathrm{C}^{N_f}_{N_p} = \sum_{N_f=1}^{N_{f,max}} \frac{N_p!}{(N_p - N_f)!N_f!}. \tag{7}$$

It should be noted that redundancy-based fault detection can detect a maximum of $N_{f,max} \leq N - M$ faults with integrity. $N_{f,max}$ can be computed according to the integrity requirements and the a priori probability of faults as shown by [10]. Hypothesis grouping methods leverage the fact that the probability of occurrence of a fault mode upper-bounds its integrity risk contribution. Thus, in satellite navigation, the

probability of occurrence of a large number of simultaneous faults (e.g., three or more simultaneous failures) is so tiny that it can directly be subtracted from the total integrity budget. An exhaustive account of all fault modes is therefore achievable. However, in multi-sensor fusion, the total number of measurements N is much larger. In addition, the rate of occurrence of outliers for some sensors and sensor algorithm is significantly higher than in satellite navigation. Moreover, operation environment of applications in urban areas increases the chance of outlier occurrence. As a result, the maximum number of faults to be monitored and the value of N_{mode} increases. Table I shows the change of $N_{f,max}$ and N_{mode} as the integrity requirements vary. In the table, the total number of measurements is $N = 30$ and the prior probability of a single measurement is set to 0.01, which can be a realistic assumption for measurements from sensors such as a camera. It is shown that the total number of fault modes increases significantly as the prior outlier probability becomes higher.

TABLE I: Number of Faults to Monitor and Total Fault Modes for $N = 30, p_{prior} = 0.01$

IR_{max}	10^{-5}	10^{-6}	10^{-7}	10^{-8}
$N_{f,max}$	5	5	6	7
N_{mode}	174436	174436	768211	2804011

It can be seen from this simple example that the explosion in complexity has limited the usage of the state-of-the-art MHSS based integrity monitoring algorithm in some multi-sensor navigation scenarios.

III. Integrity Analysis of Greedy-FDE for Multi-sensor Navigation

A. Background on Greedy-FDE

In order to monitor the integrity with limited computational power, Blanch et al. proposed a greedy search based fast FDE method in [6] for GNSS integrity monitoring. The Greedy-FDE method applies residual based test statistic:

$$\gamma = \mathbf{z}^T \mathbf{A} \mathbf{z} \tag{8}$$

with

$$\mathbf{A} = \mathbf{W}(\mathbf{I} - \mathbf{H}\mathbf{S}). \tag{9}$$

The test threshold is first calculated using all measurements as

$$T_0 = \chi^2_{N-M}(1 - p_{\text{FA}}), \tag{10}$$

where the false alert probability p_{FA} is calculated according to the continuity requirement.

If the statistical test is passed, then no detection is found. Otherwise, the measurement i that has the largest contribution to the test statistic is excluded by selecting

$$z_i = \arg\max_i r_i = \frac{W_{i,i}(z_i - \mathbf{g}_i^T \hat{\mathbf{x}})^2}{1 - \mathbf{g}_i^T W_{i,i} (\mathbf{H}^T \mathbf{W} \mathbf{H})^{-1} \mathbf{g}_i} \tag{11}$$

with $\mathbf{g}_i^T$ the i-th row of $\mathbf{H}$, and a new threshold is calculated with reduced number of measurements as

$$T_1 = \chi^2_{N-M-1}(1 - p_{\text{FA}}). \tag{12}$$

Such greedy search stops until the statistical test is passed or there is no more redundancy in the system.

B. Integrity Analysis of Greedy-FDE

Without loss of generality, assuming that the statistic test has been passed after removing t measurements, the probability of hazardous misleading information (HMI) is

$$p_{HMI} = p(|\hat{\mathbf{x}}_t - x| > AL, \gamma_t < T_t), \tag{13}$$

where AL is the alert limit for the states. The greedy search continues only if the fault-free hypothesis has been rejected in all past iterations. The system continuity is affected if the greedy search terminates due to insufficient redundancy.

The Greedy-FDE method exploits measurement residuals as test statistic, so the integrity analysis at the termination step is not much different from residual based integrity monitoring for multiple faults [11]. With the following hypotheses:

1) H_0: The current set of measurements are fault-free, so that $\gamma_t \sim \chi^2(N - M - t, 0)$
2) H_A: The current set of measurements contains fault, so that $\gamma_t \sim \chi^2(N - M - t, \lambda)$,

the residual test statistic γ_t is compared with the test threshold $T_t = \chi^2_{N-M-t}(1 - p_{\text{FA}})$ according to the continuity requirement. λ is the critical non-centrality parameter calculated from the given continuity requirement CR and a maximum integrity budget for the FDE process IR.

The minimal detectable bias (MDB) is the magnitude of the bias vector $\mathbf{b}$ corresponding to λ, so that the residual follows the non-central χ^2 distribution. The MDB can be calculated as

$$b_{min} = \sqrt{\frac{\lambda}{\mathbf{u}_m^T \mathbf{A} \mathbf{u}_m}} = \sqrt{\frac{\lambda}{\mathbf{u}_m^T \mathbf{W}(\mathbf{I} - \mathbf{H}\mathbf{S})\mathbf{u}_m}}, \tag{14}$$

$\mathbf{u}_m \in \mathbb{R}^N$ is a unit vector, the direction of which minimizes the impact of the bias vector on the residuals, i.e., the most challenging distribution of the measurement biases for the detector. For a general bias vector $\mathbf{b} \in \mathbb{R}^N$ with maximum $N - M$ non-zero elements, the faults in it can be detected with guaranteed maximum type I and type II error in the statistical test, if and only if $\|\mathbf{b}\|_2 \geq b_{min}$. The most challenging direction for the detector $\mathbf{u}_m$ can be found by searching for the minimum eigenvalue of

$$\mathbf{A}_k = \mathbf{D}_k^T \mathbf{A} \mathbf{D}_k, \tag{15}$$

where $\mathbf{D}_k \in \mathbb{R}^{N \times N_{f,k}}$ is the selection matrix corresponding to the fault mode k that selects the $N_{f,k}$ non-zero entries of the bias vector ($\|\mathbf{u}_k\|_0 = N_{f,k}$). $\mathbf{A}_k$ is full-rank since the matrix $\mathbf{A}$ has rank $N - M \geq N_{f,k}$ for all fault modes. $\mathbf{u}_m$ is the eigenvector corresponding to the minimum eigenvalue for all k.

The least detectable bias direction does not necessarily lead to largest errors in estimated states. The estimate error induced by undetected bias can be overbounded by

$$\|\mathbf{e}_{b,i}\|_2^2 = \mathbf{b}^T \mathbf{s}_i \mathbf{s}_i^T \mathbf{b} \leq \lambda \frac{\mathbf{u}^T \mathbf{s}_i \mathbf{s}_i^T \mathbf{u}}{\mathbf{u}^T \mathbf{A} \mathbf{u}}, \tag{16}$$

where $\mathbf{s}_i^T$ is the i-the row of $\mathbf{S}$ in Eqn. (6). As shown in earlier works [11], [12], the worst fault direction that causes largest integrity risk $\mathbf{u}_w$ is the bias direction that maximizes the failure mode slope, i.e.,

$$\mathbf{u}_w = \arg\max_{\mathbf{u}} \frac{\mathbf{u}^T \mathbf{s}_i \mathbf{s}_i^T \mathbf{u}}{\mathbf{u}^T \mathbf{A} \mathbf{u}}. \tag{17}$$

Joerger et al. proposed in [12] an analytical way of calculating the worst bias direction $\mathbf{u}_{w,k}$ as well as the failure mode slope under fault mode hypotheses k as

$$\mathbf{u}_{w,k} = \mathbf{D}_k \mathbf{A}_k^{-1} \mathbf{D}_k^T \mathbf{s}_i, \tag{18}$$

$$\mathbf{g}_k^2 = \mathbf{s}_i^T \mathbf{D}_k \mathbf{A}_k^{-1} \mathbf{D}_k^T \mathbf{s}_i = \mathbf{s}_i^T \mathbf{u}_{w,k}. \tag{19}$$

Then $\mathbf{u}_w$ can be selected as the direction corresponding to the largest $\mathbf{g}_k^2$ as

$$\mathbf{u}_w = \arg\max_{\mathbf{u}_{w,k}} \mathbf{s}_i^T \mathbf{u}_{w,k}. \tag{20}$$

With the worst bias direction, the maximum position error induced by the undetected bias can be calculated as

$$\bar{e}_{b,i} = \sqrt{\lambda \mathbf{s}_i^T \mathbf{u}_w}, \tag{21}$$

which should be considered when calculating protection level of the navigation system.

It should be mentioned that in order to calculate the worst slope and the corresponding error bound, Greedy-FDE still need to search over all the fault modes. Developing methods to reduce its computational cost is an important work to investigate in future.

IV. Potential Numerical Issue for Greedy-FDE in Multi-sensor Navigation

In multi-sensor navigation context, the structure and the numerical values of the Jacobian matrices from different sensors $\mathbf{J}_{s_k}$ can be significantly different. For GNSS measurements, each row of the Jacobian matrix has the structure like $\left[\frac{(\mathbf{x}-\mathbf{x}_{sat}^i)^T}{\|\mathbf{x}-\mathbf{x}_{sat}^i\|_2}, 1\right]$. The first three columns is the direction vector pointing from the satellite to the receiver, and the last column corresponds to the receiver clock offset (here only the four basic states for single constellation GNSS are mentioned for simplicity). For camera measurements, some values in the intrinsic matrix $\mathbf{K}$ in Eqn. (5) are in unit of pixel, and the values can be large for high-resolution cameras. As a result, such variety in Jacobians from different sensors leads to specific structure of the integrated geometry matrix $\mathbf{H}$. More specifically, some columns of $\mathbf{H}$ may contain large values from the camera Jacobian that are two or three orders of magnitude greater than the values from the GNSS Jacobian. As a result, that column will have a quasi-sparse structure with a few large entries and other tiny elements (relative to the large-valued entries).

After a few measurements are excluded as potential faults by multi-sensor Greedy-FDE, there may be some particular state corresponding to the column $\mathbf{h}_j$ with the aforementioned quasi-sparse structure. If the number of large values in $\mathbf{h}_j$ equals to maximum number of monitored faults $N_{f,max}$, the geometry becomes ill-conditioned for the fault detector. In such cases, there is actually no redundancy to further detect faults. Although the tightly coupled sensor fusion should provide sufficient redundancy in that state in theory, the variety in the magnitude of numerical values from different sensors reduces the significance of such redundancy. As a result, the detector will have a large MDB which degrades the availability, or the greedy search will be terminated due to insufficient degrees of redundancy so that the continuity is affected. An example of such numeric effects is shown in simulation in Section V. The solution to the issue may require reparameterizing some sensors' measurement equation to reduce the magnitude difference in the multi-sensor Jacobian matrix.

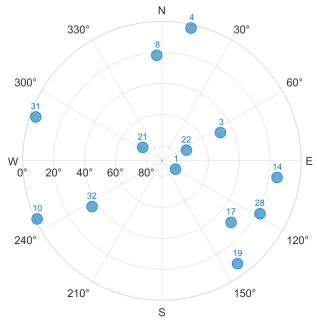

Fig. 2: Skyplot of the satellites used in simulation

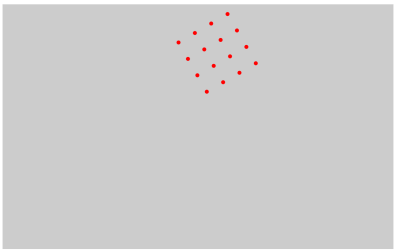

Fig. 3: Simulated image. Red dots denotes the corner points of the marker.

V. Simulation Results

In this section, a simulation scenario is set up to validate the performance of Greedy-FDE and its integrity aspects. Fig. 1 shows the simulated unmanned aerial vehicle (UAV) landing scenario. The UAV is assumed to be equipped with a GNSS receiver and a calibrated camera. The camera is downward-facing and a georeferenced visual marker on the ground is detected for visual positioning. In the simulation, it is assumed that the 16 reference corners of the markers are used as 2D feature points for the camera (in total 32 visual measurements) and 13 pseudorange measurements are generated using realistic geometry extracted from real measurement data. The skyplot of the satellite geometry is shown in Fig. 2. The relative pose between the camera and the visual marker is shown in Fig. 1.

In total there are $N = 45$ measurements (32 marker coordinates and 13 GNSS pseudoranges), and the state space has $M = 4$ dimensions (single constellation), which consists

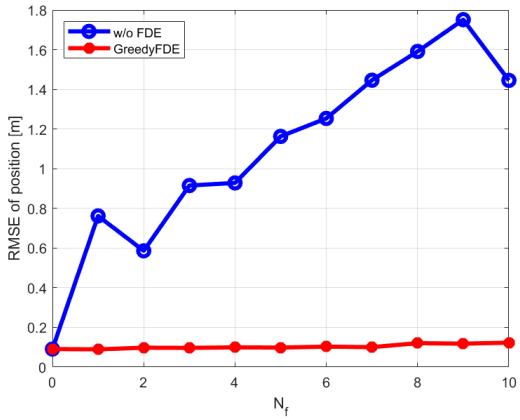

Fig. 4: Root Mean Square Error (RMSE) of Greedy-FDE for different numbers of faults

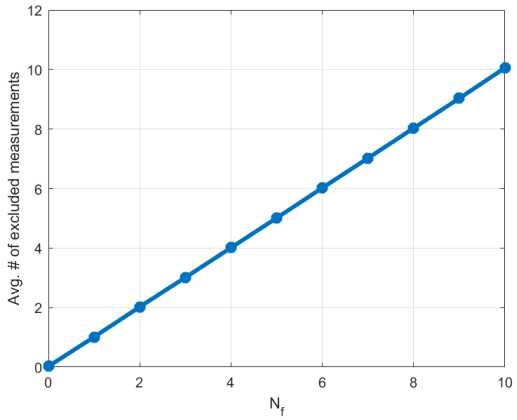

Fig. 5: Average number of exclusion using Greedy-FDE for different numbers of faults

of 3D position in local reference frame and a clock offset of the GNSS receiver. The fault detector is able to detect up to $N-M=41$ single-measurement outliers in theory. The UAV is set to be 10 meters above the ground. The noise standard deviation is assumed to be 1 [m] for GNSS and 5 [pixel] for simplicity. With the simulation set-up, the geometry matrix of the multi-sensor system can be expressed as $\mathbf{H}=\begin{bmatrix}\mathbf{J}_{GNSS}\\ \mathbf{J}_{cam}\end{bmatrix}\in\mathbb{R}^{N}$, which includes Jacobian matrices from both sensors.

Fig. 4 shows the performance improvement by applying Greedy-FDE. In this example, the norm of the bias vector is set as 200. The biases are added in the direction that at most 1 satellite (PRN1) is faulty and all the other faulty measurements are from the camera (exact direction dependent varies with the numbers of fault). It can be seen that with the FDE process, faulty measurements are removed even with a large number of faults. Consequently, the position estimation error is significantly reduced compared to no FDE case. Fig. 5 illustrates the average number of excluded measurements using Greedy-FDE in the simulation runs. It can be seen that the algorithm excludes almost exact number of faulty measurements. The number of mistakenly excluded measurements is so low that it is not easy to observe from the curve. As a quantitative example, wrong exclusion only happened 28 times in 10^4 runs for $N_f=10$, and the continuity was never lost in the simulation. The comparison of the nominal performance between Greedy-FDE and other FDE methods can be found in the original paper from Blanch et al. [6]. It should be noted that the Greedy-FDE cannot outperform the MHSS in terms of RMSE due to its suboptimal nature. However, the computational cost of MHSS based methods will be too high for most onboard computers to afford as N_f grows. A runtime comparison can be found in [8].

Fig. 6 shows the impacts of bias magnitude on positioning performance. Larger bias values facilitate FDE and therefore cause smaller positioning errors as compared to smaller fault magnitudes. Smaller faults cannot always be detected if the bias magnitude is lower than the minimal detectable

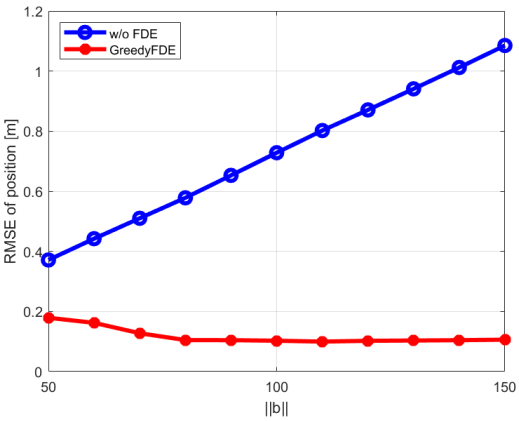

Fig. 6: Impact of bias magnitude on RMSE. b_{min}=97.8621, N_f=7.

bias. This result consolidates the MDB calculation. For such geometry in the example scenario, the MDB value is MDB=97.8621. Simulated biases are added to 7 measurements with the worst distributed direction $\mathbf{u}_m$. As the magnitude of the bias changes from below the MDB to larger than MDB, the detectability of the faults changes significantly. This can also be seen from the average number of excluded measurements in Fig. 7 and from the miss detection rate curve in Fig. 8.

Additionally, an example of the numerical issue discussed in Section IV is provided. The system setup contains a total of 21 measurements including 6 feature points (12 measurements) and 9 satellites. The magnitude value of $\mathbf{H}$ is illustrated in Fig. 9. In the plot, the x and y axes indicate the column and row indices of elements of the $\mathbf{H}$ matrix. The color of each cell reflects the magnitude of the numeric value of the corresponding matrix element. Here, the values are normalized using the maximum number in the $\mathbf{H}$ matrix so that the values are in the range [0,1]. It can be seen that in the first two columns, there are 6 elements with large value (with value around 139 before normalization) and the other values are very small (for the first columns all below 1 even without normalization). This shows that the first column

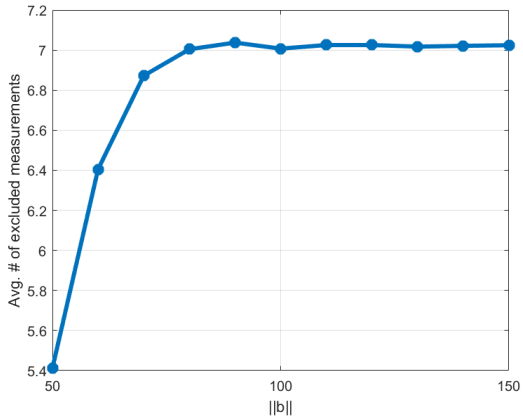

Fig. 7: Average number of exclusion using Greedy-FDE for different magnitude of bias

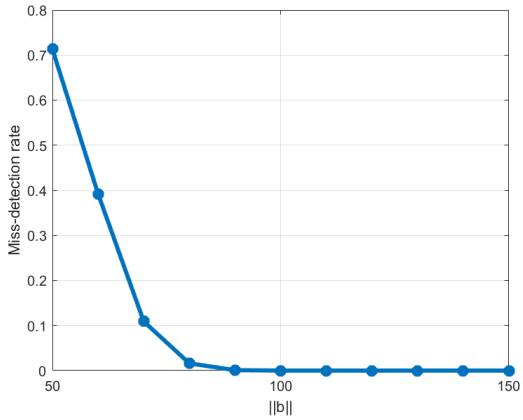

Fig. 8: Miss detection rate for different bias magnitude. $IR = 10^{-8}, CR = 1\%$

of the geometry matrix has a quasi-sparse structure due to numerical effects from different sensors. The reason for the significant difference in the values is that the intrinsic matrix $\mathbf{K}$ in Eqn. (5) contains values as large as a few hundreds that propagates to the Jacobian $\mathbf{J}_{cam}$ and other values in the same column of the Jacobian are zero or small numbers below one. In such case, the system losses redundancy and the Greedy-FDE will be interrupted.

VI. Conclusion and Outlook

In the context of multi-sensor navigation, greedy search based FDE needs to be used in the scenarios when the computational complexity of solution separation method is too high. The Greedy-FDE relies on the residual based statistical test to detect outliers. The integrity of the method is analyzed, with a focus point on the minimal detectable bias and worst case slope calculation. It has been validated that Greedy-FDE is efficient and effective for integrity monitoring with a large number of faults. Nevertheless, the calculation of the worst case slope still require to search over all fault modes. Innovative methods to reduce its computational complexity is demanded in future developments. There are also potential corner cases due to numerical issues from multi-sensor fusion. The appearance possibility of such events in real life is yet to be further investigated in future work.

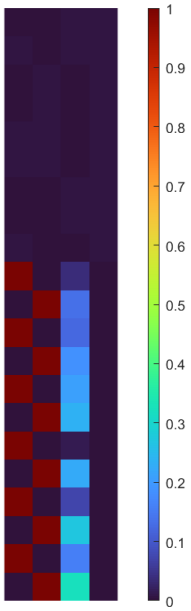

Fig. 9: Illustration of the magnitude of $\mathbf{H}$

References

[1] M. Joerger and B. Pervan, "Quantifying safety of laser-based navigation," *IEEE Transactions on Aerospace and Electronic Systems*, vol. 55, no. 1, pp. 273–288, 2019.

[2] C. Zhu, M. Meurer, and C. Günther, "Integrity of visual navigation - developments, challenges, and prospects," *NAVIGATION: Journal of the Institute of Navigation*, vol. 69, no. 2, 2022.

[3] M. Brenner, "Integrated gps/inertial fault detection availability," *NAVIGATION*, vol. 43, no. 2, pp. 111–130, 1996. [Online]. Available: https://onlinelibrary.wiley.com/doi/abs/10.1002/j.2161-4296.1996.tb01920.x

[4] B. S. Pervan, S. P. Pullen, and J. R. Christie, "A multiple hypothesis approach to satellite navigation integrity," *NAVIGATION*, vol. 45, no. 1, pp. 61–71, 1998. [Online]. Available: https://onlinelibrary.wiley.com/doi/abs/10.1002/j.2161-4296.1998.tb02372.x

[5] J. Blanch, T. Walker, P. Enge, Y. Lee, B. Pervan, M. Rippl, A. Spletter, and V. Kropp, "Baseline advanced raim user algorithm and possible improvements," *IEEE Transactions on Aerospace and Electronic Systems*, vol. 51, no. 1, pp. 713–732, 2015.

[6] J. Blanch, T. Walter, and P. Enge, "Fast multiple fault exclusion with a large number of measurements," in *Proceedings of the 2015 International Technical Meeting of the Institute of Navigation*, 2015, pp. 696–701.

[7] J. Wendel, "Gnss pseudorange fault detection and exclusion with multiple outliers," in *Proceedings of the 35th International Technical Meeting of the Satellite Division of The Institute of Navigation (ION GNSS+ 2022)*, 2022, pp. 1481–1495.

[8] C. Zhu, M. B. Takim, and M. Meurer, "Greedy algorithm based integrity monitoring for visual navigation," in *Navigation 2021 (combined conference ENC2021 and INC2021), Edingburgh, UK*, 2021.

[9] J. J. Moré, "The levenberg-marquardt algorithm: implementation and theory," in *Numerical analysis*. Springer, 1978, pp. 105–116.

[10] M. Joerger, F.-C. Chan, S. Langel, and B. Pervan, "Raim detector and estimator design to minimize the integrity risk," in *Proceedings of the 25th International Technical Meeting of the Satellite Division of the Institute of Navigation (ION GNSS 2012)*, 2012, pp. 2785–2807.

[11] J. E. Angus, "Raim with multiple faults," *Navigation*, vol. 53, no. 4, pp. 249–257, 2006.

[12] M. Joerger, F.-C. Chan, and B. Pervan, "Solution separation versus residual-based raim," *NAVIGATION*, vol. 61, no. 4, pp. 273–291, 2014. [Online]. Available: https://onlinelibrary.wiley.com/doi/abs/10.1002/navi.71